Efficient removal of antibiotics from water via aqueous portlandite carbonation

German Montes-Hernandez, L. Feugueur, C. Vernier, A.E.S. van Driessche, F. Renard

Efficient Removal of Antibiotics from Water via Aqueous Portlandite Carbonation

G. Montes-Hernandez[a] *, L. Feugueur[a], C. Vernier[a], A.E.S. Van Driessche[a,b], F. Renard[a,c]

[a] ISTerre, Univ. Grenoble Alpes, Grenoble INP, Univ. Savoie Mont Blanc, CNRS, IRD, Univ. Gustave Eiffel, 38000 Grenoble, France

[b] Instituto Andaluz de Ciencias de la Tierra (IACT), CSIC – University of Granada, Armilla, Granada E-18100, Spain

[c] The Njord Centre, Departments of Geosciences and Physics, University of Oslo, Norway

*Corresponding author: Dr. German Montes-Hernandez

E-mail address: german.montes-hernandez@univ-grenoble-alpes.fr

Abstract

Current wastewater treatment technologies struggle to remove antibiotics from wastewaters, leading to contamination of surface and groundwater. Therefore, more effective and efficient processes for removing antibiotics from water are needed. The present study reports for the first time that three widely used antibiotics (amoxicillin, ceftriaxone, cefazoline) can be successfully removed from water under ambient conditions by using aqueous carbonation of portlandite. Breakthrough curves acquired from flow-through experiments and their respective removal isotherms were mainly used to determine quantitative equilibrium parameters. In this way, the removal of antibiotics using aqueous portlandite carbonation is very efficient for amoxicillin (9.5 mg/g), followed by cefazoline (4.3 mg/g) and ceftriaxone (2.7 mg/g). In a comparison perspective, nanomagnetite-interfacial Fenton reaction is more effective in removing amoxicillin (76.5 mg/g); however, the process is slower and chemically more complex. However, both investigated methods offer promising results at the laboratory scale and are technically feasible to be implemented in conventional and/or advanced wastewater treatment plants.

Keywords: Antibiotic, Removal, Wastewater, Carbonation, Portlandite, Magnetite, Flow-through curves, Isotherms

1. Introduction

De novo designed organic molecules, including pharmaceuticals, hormones, personal care products, surfactants, drugs, and pesticides, are a serious source of contaminants in water. Among these pollutants are antibiotics, the most frequently prescribed drug of modern human medicine, which are also widely used in the animal farming industry, including cattle, swine, poultry, and fish. The benefits of antibiotics in healthcare of human and animals are undisputed. However, excessive and wrong usage raises the risk of drug resistance in the environment, leading to the most common antibiotics being no longer effective in controlling infectious diseases [1-5]. Antibiotics from different sources (e.g. municipal waste water, hospitals, animal production, and pharmaceutical industries) are ultimately discharged into wastewater treatment plants. However, conventional and advanced treatment plants are not effective in removing antibiotics leading to the release of these compounds in surface and groundwater [6-7]. In the last two decades, various methods to remove and/or degrade antibiotics from water have been investigated in the laboratory and frequently tested in pilot or plant scale, including biodegradation, nanofiltration, advanced oxidation processes, photocatalytic degradation, reverse osmosis, ozonation and adsorption [8-15]. Among these methods, adsorption appears to be a suitable technique to remove various antibiotics from contaminated water and industrial effluents because of its high efficiency, simple design, easy operation and its ability to remove a wide range of contaminant concentrations. High specific surface areas (>500 m^2/g) and microporous materials (e.g. metal–organic frameworks – MOFs) are frequently required; but in general, diversified natural or synthetic materials (including green and low-cost materials) have been tested to remove antibiotics [16-18]. Mineral precipitation has also been suggested as an economic and robust method to remove ionic and organic pollutants from water; for example, calcite precipitation can remove several heavy metals and metalloids from

66 water, but rarely organic pollutants [19-20].

67 In the present study we show that calcite precipitation via aqueous portlandite carbonation
68 ($Ca(OH)_2 + CO_2 \Rightarrow CaCO_3 + H_2O$) in a flow-through reactor at ambient conditions is a simple
69 method to effectively remove three types of antibiotics (amoxicillin, ceftriaxone and cefazolin).
70 This carbonation method has been investigated in order to produce nanosized calcite under mild
71 and hydrothermal conditions or in order to sequester ionic pollutants from water [19-20]. In this
72 way, based on breakthrough curves and respective sequestration isotherms we establish the
73 efficiency of this approach. In addition, we show, using the same flow-through setup, that a Fenton-
74 type oxidation reaction using magnetite nanoparticles is also an efficient process to remove
75 amoxicillin. However, this oxidation reaction requires low pH (pH<3), a significant amount of
76 oxygenated water and a ferrous source (Fe(II) as enhancing reaction agents.

77

78 **2. Materials and Methods**

79 *2.1. Chemicals*

80 Four antibiotics (amoxicillin ($C_{16}H_{19}N_3O_5S$), erythromycin ($C_{37}H_{67}NO_{13}$), ceftriaxone
81 ($C_{18}H_{18}N_8O_7S_3$), cefazolin ($C_{14}H_{14}N_8O_4S_3$)) and soluble salts (calcium chloride dihydrate
82 ($CaCl_2.2H_2O$), ferrous chloride dihydrate ($FeCl_2.2H_2O$), ferric chloride heptahydrate ($FeCl_3.6$
83 H_2O) and sodium hydroxide (NaOH)) with high purity (>99%) were obtained from Sigma-Aldrich.
84 All reactants were used as received. Carbon dioxide (CO_2) was obtained from Linde Gas S.A. with
85 99.995% of chemical purity. This gas was used as received and directly bubbled into the antibiotic
86 inlet solutions. Deionized water (18.2 MΩ of resistivity) used in the synthesis of minerals, drinking
87 water of the city of Grenoble (its ionic composition and/or chemistry was already reported in a
88 previous study [21]) used in flow-through and batch experiments and oxygenated water (H_2O_2) at

30% (provided by Sigma-Aldrich) and chloride acid (HCl) at 10% (provided by Sigma-Aldrich) used in the Fenton's reaction.

2.2. Minerals

Portlandite platy nanoparticles ($Ca(OH)_2$ with hexagonal shape and with 16 m^2/g of specific surface area) were synthesized using a coprecipitation method in alkaline medium ($Ca^{2+} + 2OH^- \Rightarrow Ca(OH)_2$) by rapid mixing of 100 ml of calcium chloride solution (1 M) with 210 ml of sodium hydroxide (1 M) at room temperature. The resulting suspension was stirred for 15 minutes and then the precipitate was recovered by filtration and washed with deionized water. Finally, the portlandite was dried in a CO_2-free atmosphere at 60 °C for 24 h.

Magnetite spherical nanoparticles (Fe_3O_4 with size<20nm, with 28 m^2/g of specific surface area) were synthesized using a coprecipitation method by adding 200 ml of a mixed-valent iron solution (1 M, ($Fe^{2+} + Fe^{3+}$), pH ~ 1) with a controlled flow rate (2.3 ml/min) to 200 ml of NaOH solution (4 M, pH = 14) at room temperature under constant stirring. The reaction mechanism and kinetics for this coprecipitation reaction have been previously investigated by time-resolved Raman spectroscopy [22].

Calcite nanoparticles ($CaCO_3$ with size<100nm, with 9 m^2/g of specific surface area) was synthesized by aqueous carbonation of portlandite with compressed CO_2 (55 bar) at room temperature, following the overall reaction: $Ca(OH)_2 + CO_2 \Rightarrow CaCO_3 + H_2O$. The mineral composition, kinetics, and reaction mechanisms were determined by time-resolved Raman spectroscopy measurement [23].

111 *2.3. Flow-through reactor experiments*

112 *Aqueous carbonation of portlandite*: Two flow-through reactors with 50 mL internal volume were
113 first filled with Grenoble drinking water, ionic composition reported in Hajji et al. [21]. One reactor
114 also contained 1 g of synthetic portlandite (reactive tracer reactor). The other reactor without
115 mineral-reactant was used as a reference (inert tracer reactor). An antibiotic-rich solution (2 L with
116 100-120 mg/L of a given antibiotic) was constantly bubbled with CO_2 in a beaker. Then, this CO_2-
117 saturated antibiotic solution was simultaneously percolated through both reactors at a constant rate
118 of 12.2 mL/min for 80 minutes at room temperature (20 °C). The mineral-solution suspension in
119 the flow-through reactor was continuously stirred using a magnetic Teflon bar. The outflow
120 solutions from the inert and reactive tracer reactors were filtered in situ through 0.2 µm pore size
121 Teflon membranes located on the top of the reactors. The antibiotic concentration in filtered
122 solutions at various times of the experiment (0.5, 2, 5, 10, 15, 20, 80 minutes) were determined
123 with Ultraviolet-Visible (UV-Vis) spectroscopy (Agilent Cary 60). We used calibration lines for
124 amoxicillin ($C_{amoxicillin}$=A/0.0216) at 228 nm (where C is concentration and A is the absorbance),
125 ceftriaxone ($C_{ceftriaxone}$=A/0.0444) at 237 nm and cefazolin ($C_{cefazolin}$=A/0.0236) at 273nm. These
126 measurements were used to determine experimental breakthrough curves for the solutions of the
127 inert and reactive tracer reactors, as previously described for As and Cr sequestration by using
128 nanostructured synthetic minerals [21]. All experiments were repeated at least two times in order
129 to confirm their reproducibility.

130

131 *Fenton reaction*: The same experimental setup as described above was used to investigate the
132 oxidation process of amoxicillin. Here, 1 g of magnetite nanoparticles was placed in the reactive
133 tracer reactor and provided a ferrous iron source for the Fenton reaction at the magnetite-solution

interfaces. The inlet solution containing amoxicillin (2 L with 120 mg/L) was modified to activate the Fenton reaction by adding 1.2 ml of 30% oxygenated water (H_2O_2) and adjusting the pH to 2.6 by adding HCl. This solution was simultaneously flown through both (inert and reactive) reactors at a rate of 2.3 ml/min during 7 hours. Solution samples were retrieved at different time intervals (outlet solutions from inert and reactive tracer reactors) and analyzed by UV-Vis spectroscopy in order to measure the evolution of the amoxicillin concentration and determine the respective breakthrough curves.

Calculation of removal isotherms: The experimental breakthrough curves obtained from the inert and reactive tracer reactors were used to determine the removal isotherm for a given antibiotic. The corresponding removed fraction between C=0 and C_i was calculated by integrating the surface area between the breakthrough curves of the inert and reactive tracers inside of a given interval of time. Each of these calculations provided one point (C_i, q_i) of the isotherm; assuming an equilibrium concentration in each point as explained in Limousin et al. [24]. The relationship to determine the removed amount (q_i=q_e) for a given equilibrium concentration (C_i=C_e) from breakthrough curves writes as follows:

$$q_i = \frac{\text{Flow rate}}{\text{Solid mass}} A_i = \frac{\text{Flow rate}}{\text{Solid mass}} \left(\int_{t=0}^{t=t_i} C_{\text{inert tracer}}\ dt - \int_{t=0}^{t=t_i} C_{\text{reactive tracer}}\ dt \right) \quad (1)$$

The main advantage of this method is that only one percolation experiment for inert and reactive tracer reactors is required to determine one isotherm for a given pollutant. Finally, all removal isotherms obtained from breakthrough curves were fitted using Hill's model ($q_e = \frac{q_{e(\max)} C_e^b}{K^b + C_e^b}$ with $q_{e(max)}$, K and b fitting parameters) than can describe sigmoidal complex behaviors, and, in several cases, is equivalent to the Langmuir adsorption model.

156

157 *2.4. Batch reactor experiments*

158 Aqueous carbonation of portlandite in the presence of antibiotic was also monitored in real time
159 with Raman spectroscopy in order to identify the effect of antibiotics on the nucleation process of
160 calcite. Here, 2 g of synthetic portlandite was dispersed in 200 ml of an antibiotic solution (100
161 mg/L) placed inside of a hydrothermal reactor equipped with an in-situ Raman probe (RAMAN
162 RXN1, Kaiser Optical Systems). Then, 5-10 bar of CO_2 was injected in the reactor and the system
163 was monitored during 20-60 minutes at a rate of one acquisition every 0.25 or 1 min. This custom-
164 build experimental setup has been used to investigate the nucleation, growth and transformation of
165 several mineral phases [23, 25-27].

166 For the Fenton reaction, two additional experiments were performed using 2 L beakers. Here, 1 L
167 of amoxicillin solution (130 mg/L, 0.6 ml of oxygenated water at pH=2.55) was stirred in the
168 presence of 1 g of magnetite nanoparticles. Several fluid samples were withdrawn at different time
169 intervals and the amoxicillin concentration was determined with UV-Vis spectroscopy.

170

171 *2.5. Ex situ characterization of solids*

172 Selected recovered solid samples were dried under air atmosphere at 60 °C for 48 h and stored in
173 plastic flasks for subsequent characterization by Field-Emission Scanning Electron Microscopy
174 (FESEM) and powder X-ray diffraction (PXRD).

175 XRD patterns were acquired using a Siemens D5000 diffractometer in Bragg-Brentano geometry,
176 equipped with a theta-theta goniometer with a rotating sample holder. Diffraction patterns were
177 then collected using Cu kα_1 ($\lambda_{k\alpha1}$=1.5406 Å) and Cu kα_2 ($\lambda_{k\alpha2}$=1.5444 Å) radiations in the range

178 2θ = 10 - 70°, with a step size of 0.04° and a counting time of six seconds per step. Coherent
179 average size of some samples was systematically refined by the quantitative Rietveld method on
180 XRD patterns using the BGMN software and its associated database [28].
181 Concerning the high-resolution microscopy imaging, the solid products were dispersed by
182 ultrasonic treatment in high purity water for five minutes. One droplet of the suspension was then
183 deposited directly on an aluminum support and observed without metal coating because calcite and
184 magnetite nanoparticles have enough conductivity. The powder was imaged using a Zeiss Ultra 55
185 FESEM with a maximum spatial resolution of ca. 1 nm at 15 kV.
186
187 **3. Results and discussion**
188 *3.1. Removal of antibiotics by portlandite aqueous carbonation*
189 During a representative carbonation reaction of portlandite ($Ca(OH)_2$) in a CO_2-saturated solution,
190 first the portlandite particles dissolve and release Ca^{2+}. Immediately, amorphous calcium carbonate
191 (ACC) particles precipitate, and transform into calcite ($CaCO_3$) within a few seconds to minutes,
192 as demonstrated by previous time-resolved Raman spectroscopy measurements [23]. In this way,
193 the calcite growth process can incorporate, adsorb and/or enhance precipitation of ionic elements
194 (Se, As, Cr, Fe, Mn, Sb, P and N) from polluted solutions, [19-20, 29-35] and also remove organic
195 pollutants such as antibiotics as demonstrated in the present study.
196 Herein, we assessed the efficiency of the antibiotic removal via aqueous portlandite carbonation
197 by comparing breakthrough curves obtained simultaneously from the inert and reactive tracer
198 reactors. In our experimental setup, if the pollutant does not have any physiochemical affinity
199 and/or reactivity with the dispersed solid particles, the breakthrough curves for inert and reactive
200 tracers should overlap. However, if some interaction with the dispersed particles occurs, the

breakthrough curve for the reactive tracer may display a significant retarding effect with respect to the breakthrough curve of the inert tracer. In such case, a removal isotherm can be calculated by using Eq. 1. Figures 1 and 2 show breakthrough curves and removal isotherms for amoxicillin in the presence of different starting amounts of portlandite. These curves reveal that a significant amount of amoxicillin is removed during aqueous carbonation of portlandite. This process is directly related to initial available portlandite (1 or 2 g). The retarding of reactive tracer curve is also proportional to the initial dose (see breakthrough curves in Figures 1 and 2). These results thus show that amoxicillin is sequestered during the carbonation process of portlandite, i.e. when calcite is forming. A control experiment was performed where high purity calcite was used as potential sequestration agent. In this case, breakthrough curves for inert and reactive tracers overlap (see Fig. SI-1), indicating negligible amoxicillin sorption/sequestration onto already formed calcite particles. This result thus further confirms that amoxicillin is being retained from solution during the initial stages of calcite formation.

The removal isotherms for amoxicillin, i.e. the removed amount as a function of equilibrium concentration, are equivalent when 1 or 2 g of portlandite are used (Figures 1 and 2 on the right). This result is consistent because the removed amount of amoxicillin was normalized with portlandite mass and an equilibrium concentration in the percolating solution was assumed in these flow-through experiments. Specifically, the fitted parameters from Hill's model show that the equilibrium constant K (equilibrium concentration, which represents also the half-removed amount of pollutants), the maximum removed amount, $q_{e(max)}$, and Hill's coefficient, b, are equivalent for both initial quantities of portlandite. K and $q_{e(max)}$ are two fundamental parameters to calculate the liquid-solid distribution coefficients ($K_D = q_{e(max)}/K$, given in [L/g]). K_D is widely used to simulate the mass transfer at the solid-fluid interfaces in porous media [19]. Table 1 provides these

parameters for all fitted isotherms.

The removal of two other antibiotics (ceftriaxone and cefazolin) was also assessed. Figures 3 and 4 show the breakthrough curves and the removal isotherms for cefazolin and ceftriaxone, respectively. These data show that both antibiotics are also efficiently removed from solution by aqueous carbonation of portlandite. The removed amount versus equilibrium concentration follows a similar trend for both antibiotics and the removal isotherms were again fitted using Hill's model (Table 1). In summary, significant amounts of amoxicillin, ceftriaxone, and cefazoline can be removed by aqueous carbonation of portlandite. The plateaus in the isotherm curves of Figures 1, 2, 3, and 4 (on the right) show that the method is most efficient for amoxicillin (9.5 mg/g), followed by cefazoline (4.3 mg/g) and ceftriaxone (2.7 mg/g). Erythromycin was also assessed, unfortunately, this antibiotic has low absorbance in UV vis spectroscopy at the investigated concentration. For this reason, only qualitative results are commented in the following paragraphs. Noteworthy, the UV-Vis spectroscopy data reveal that the absorbance peak for amoxicillin, cefazoline and ceftriaxone shifts to a higher wavelength in portlandite alkaline media. For example, amoxicillin absorbance shifts from 228 nm (typical in water) to 247 nm in a saturated portlandite solution (Fig. SI-2). This is probably due to a strong complexation of amoxicillin with Ca^{2+} in an alkaline solution because such peak shifts back to typical absorbance wavelength in water (i.e. 228 nm) when all portlandite was consumed in the system, i.e. when calcite precipitation had finished during a percolation experiment. The observed shifts also agree with a complexation study of amoxicillin in Ca^{2+} systems [36]. The UV-Vis time-resolved spectra during amoxicillin removal by portlandite aqueous carbonation (Fig. 5) may be explained by a selective Ca complexation of this antibiotic under alkaline conditions, a process which could also contribute to antibiotic removal.

To gain insight on the influence of antibiotic on the nucleation of calcite from aqueous carbonation of portlandite additional batch experiments were performed in real time using Raman spectroscopy. Results show that the presence of antibiotics does not change significantly the calcite nucleation mechanism. Amorphous calcium carbonate peaking at 1080 cm^{-1} was detected as the only transient phase and its lifetime varied slightly with the different antibiotics in the range three to five minutes under our experimental conditions (Fig. 6).

FESEM images acquired on the recovered solid phase showed oriented aggregates of calcite crystals (resembling mesocrystals) for all antibiotics, except erythromycin where well-dispersed nanoparticles of calcite were obtained (see Fig. SI-3). Average calcite particle sizes observed in FESEM images agree with the average particle size extracted from powder XRD patterns. In particular, the average particle size for calcite varies when a given antibiotic is used, as revealed by the full wide half maximum (FWHM) parameter. The position of the main reflection (104) varies also slightly, which is probably due to a minor incorporation of the antibiotic into the calcite crystal lattice (see Fig. SI-4).

Our spectroscopic and textural data suggest that complexed antibiotic was mainly removed during the formation and transformation of amorphous calcium carbonate (ACC) into calcite. We interpret that the organic material adhered onto calcite nanoparticles, inducing the formation of mesocrystals, a process that was previously observed during calcite formation via aqueous carbonation of portlandite in presence of common domestic drinks [37].

3.2. Removal of amoxicillin by Fenton reaction

Advanced oxidation of organic pollutants via the so-called Fenton process has been investigated and implemented in modern wastewater plant treatment [38]. For this reason, we investigate here

a modified Fenton reaction using nanosized magnetite as ferrous source for amoxicillin removal, in order to compare it with the aqueous carbonation of portlandite method. A typical Fenton oxidation process involves complex redox and decomposition reactions between several reactants (ferrous iron, oxygenated water and antibiotic) at low pH in the range 2.5-3.5. In our experiments, we varied the concentration of oxygenated water, magnetite particle size and pH adjustment. The antibiotic removal amount was exclusively obtained when the pH was pre-adjusted to 2.6 and when 260 mg/L of oxygenated water and magnetite nanoparticles were used. In this case, the amoxicillin was partially oxidized by Fenton reaction, as revealed by the breakthrough curves for inert and reactive tracers (Fig. 7). Herein, the ferrous iron was provided from surface magnetite dissolution enhanced at low pH in the presence of oxygenated water. Then the oxidation of amoxicillin took place at the surface of the magnetite nanoparticles, including two main reactions taking place at the nanoparticle-solution interface:

$$Fe^{2+} + H_2O_2 \Rightarrow Fe^{3+} + \bullet OH + OH^- \quad (2)$$

$$\text{Antibiotic} + \bullet OH \Rightarrow CO_2 + H_2O + \text{inorganic-matter} \quad (3)$$

The oxidation and/or degradation process of antibiotics can imply various intermediate steps, as determined for amoxicillin in aquatic environment [39]. In our case, a simpler approach was used by measuring the residual amoxicillin in water during flow-through experiments at different time intervals using UV-Vis spectroscopy. The breakthrough curve for the reactive tracer shown in Figure 7 reveals a significant retarding with respect to the inert tracer after seven hours of percolation and the reaction is still active because the concentration in the outlet solution has not reached the concentration of the inlet solution. This indicates that the oxidation of amoxicillin is a relatively slow process.

Importantly, the removal isotherm shown in Fig. 7 (on the right) did not reach the maximum amount of removed amoxicillin calculated by Hill's model. This model estimates a maximum removal amount of about 76 mg/g (see Table 1 and projection curve on Fig. SI-6). In order to validate this calculation, we performed several batch reactor experiments (volume 1 L). The obtained data showed that 33 mg of amoxicillin per g of magnetite nanoparticles were removed after 7-24h (Fig. SI-7). This result agrees well with the flow-through experiments and both experimental configurations indicate that the Fenton reaction was probably passivated by iron oxidation at the magnetite-solution interfaces, but such reactions remained active during several hours in flow-through and batch reactors as demonstrated in the present study. In practice, as expected the interfacial-magnetite Fenton reaction is also an efficient method to remove amoxicillin from water. But, this reaction is not active when the pH is not adjusted to 2.6; here, the amoxicillin oxidation is not active and/or negligible as revealed by an overlapping of breakthrough curves for inert and reactive tracers (Fig. SI-5). A similar inactivation of the Fenton reaction was observed at lower concentrations of oxygenated water and when microparticles of magnetite were used instead of nanoparticles.

4. Conclusion

Amoxicillin can be successfully removed from water using a flow-through setup implementing aqueous carbonation of portlandite or an interfacial-magnetite Fenton reaction. Both methods can efficiently remove these antibiotics from water as demonstrated with breakthrough curves and their respective removal isotherms. The interfacial-magnetite Fenton reaction offers a better removal capacity for amoxicillin with respect to aqueous carbonation of portlandite. Importantly, the solid-liquid separation could be facilitated because the reacting magnetite particles preserve their

magnetic potential, and this Fenton reaction can be used to remove organic pollutants from water at an industrial scale. We also assessed the removal capacity of the carbonation method for two other antibiotics, ceftriaxone and cefazoline. In overall, aqueous carbonation of portlandite offers a more promising and easier operating method to remove antibiotics from water because it can be implemented without significant modification of existing water treatment plants, for example, by using coagulation units that are already present in these plants. In our method, the treated water is neutralized with CO_2 during aqueous carbonation of portlandite and the pH at the outlet flow is close to 7. This water could be directly discharged into nature, reused, or undergo additional treatment. In addition, this method can also be used to efficiently remove ionic pollutants such as heavy metals and metalloids (e.g. As, Se and Fe). Moreover, the generated solid product, about 1.35 kg of high purity calcite per m^3 of treated water, can be re-used in a variety of industrial applications such as additive and mineral filler (e.g. plastics, paper, paintings, etc.).

Acknowledgements

The authors acknowledge funding from the French National Centre for Scientific Research (CNRS) and the Université Grenoble Alpes (UGA). We thank Nathaniel Findling for technical assistance with XRD data. The study received funding from ADEME (The French Agency for Ecological Transition) through the project FUNMIN.

Appendix A. Supplementary data

The supplementary material contains seven figures, provided in the online version, at the following web link.

References

[1] I. T. Carvalho, L. Santos, Antibiotics in the aquatic environments: A review of the European scenario, Environ. Int. 94 (2016) 736–757.

[2] M. Sagaseta de Ilurdoz, J. J. Sadhwani, V. Reboso, Antibiotic removal processes from water & wastewater for the protection of the aquatic environment - a review, J. Water Proc. Eng. 45 (2022) 102474.

[3] M. F. Li, et al., Graphene and graphene-based nanocomposites used for antibiotics removal in water treatment: A review, Chemosphere 226 (2019) 360-380.

[4] S. Zhang, W. Lin, X. Yu, Effects of full-scale advanced water treatment on antibiotic resistance genes in the Yangtze Delta area in China, FEMS Microbiol. Ecol. 92/5 (2016) fiw065.

[5] A. S. Oberoi, et al., Insights into the fate and removal of antibiotics in engineered biological treatment systems: A Critical Review, Environ. Sci. Technol. 53 (2019) 7234−7264.

[6] A. J. Watkinsona, E. J. Murbyc, S. D. Costanzo, Removal of antibiotics in conventional and advanced wastewater treatment: Implications for environmental discharge and wastewater recycling, Water Res. 41 (2007) 4164-4176.

[7] Z. Song, et al., Occurrence, fate and health risk assessment of 10 common antibiotics in two drinking water plants with different treatment processes, Sci. Total Environ. 674 (2019) 316-326.

[8] J. Yu, et al., Removal of antibiotics from aqueous solutions by a carbon adsorbent derived from protein-waste-doped biomass, ACS Omega 5 (2020) 19187-19193.

[9] Y. Z. Yan, et al., Hierarchical multi-porous carbonaceous beads prepared with nano-$CaCO_3$ in-situ encapsulated hydrogels for efficient batch and column removal of antibiotics from water, Microporous Mesoporous Mater. 293 (2020) 109830.

[10] S. R. Zhu, et al., Covalent triazine framework modified BiOBr nanoflake with enhanced

390 photocatalytic activity for antibiotic removal, Cryst. Growth Des. 18 (2018) 883-891.
391 [11] S. E. Estrada-Flórez, E. A. Serna-Galvis, R. A. Torres-Palma, Photocatalytic vs. sonochemical
392 removal of antibiotics in water: Structure degradability relationship, mineralization, antimicrobial
393 activity, and matrix effects, J. Environ. Chem. Eng. 8 (2020) 104359.
394 [12] Y. Liu, et al., Preparation of magnetic hyper-cross-Linked polymers for the efficient removal
395 of antibiotics from water, ACS Sustainable Chem. Eng. 6 (2018) 210-222.
396 [13] F. Yu, Y. Li, S. Han, J. Ma, Adsorptive removal of antibiotics from aqueous solution using
397 carbon materials, Chemosphere 153 (2016) 365-385.
398 [14] S. Jia, et al., Removal of antibiotics from water in the coexistence of suspended particles and
399 natural organic matters using amino-acid-modified-chitosan flocculants: A combined experimental
400 and theoretical study, J. Hazard. Mater. 317 (2016) 593-601.
401 [15] B. L. Phoona, et al., Conventional and emerging technologies for removal of antibiotics from
402 wastewater, J. Hazard. Mater. 400 (2020) 122961.
403 [16] H. J. Cho, et al., Impact of Zr_6 node in a metal−organic framework for adsorptive removal of
404 antibiotics from water, Inorg. Chem. 60 (2021) 16966-16976.
405 [17] J. Imanipoor, et al., Adsorption and desorption of amoxicillin antibiotic from water matrices
406 using an effective and recyclable MIL-53(Al) metal−organic framework adsorbent, J. Chem. Eng.
407 Data 66 **(**2021) 389-403.
408 [18] R. Rostamian, H. Behnejad, A unified platform for experimental and quantum mechanical
409 study of antibiotic removal from water, J. Water Proc. Eng. 17 (2017) 207-215.
410 [19] G. Montes-Hernandez, et al., Removal of oxyanions from synthetic wastewater via
411 carbonation process of calcium hydroxide: Applied and fundamental aspects, J. Hazard. Mater. 166
412 (2009)788-795.

413 [20] G. Montes-Hernandez, et al., Nanostructured calcite precipitated under hydrothermal
414 conditions in the presence of organic and inorganic selenium, Chem. Geol. 290 (2011) 109-120.
415 [21] S. Hajji, et al., Arsenite and chromate sequestration onto ferrihydrite, siderite and goethite
416 nanostructured minerals: Isotherms from flow-through reactor experiments and XAS
417 measurements, J. Hazard. Mater. 362 (2019) 358-367.
418 [22] G. Montes-Hernandez, N. Findling, F. Renard, Direct and indirect nucleation of magnetite
419 nanoparticles from solution revealed by time-resolved raman spectroscopy, Cryst. Growth Des. 21
420 (2021) 3500-3510.
421 [23] G. Montes-Hernandez, F. Renard, Time-resolved in situ Raman spectroscopy of the nucleation
422 and growth of siderite, magnesite and calcite and their precursors, Cryst. Growth Des. 16 (2016)
423 7218-7230.
424 [24] G. Limousin, et al., Sorption isotherms: A review on physical bases, modeling and
425 measurement, Appl. Geochem. 22 (2007) 249-275.
426 [25] G. Montes-Hernandez, F. Renard, Nucleation of brushite and hydroxyapatite from amorphous
427 calcium phosphate phases revealed by dynamic in situ Raman spectroscopy, J. Phys. Chem. C 124
428 (2020) 15302-15311.
429 [26] G. Montes-Hernandez, M. Bah, F. Renard, Mechanism of the formation of engineered
430 magnesite: A useful mineral to mitigate CO_2 industrial emissions, J. CO2 Util. 35 (2020) 272-276.
431 [27] G. Montes-Hernandez, et al., Amorphous calcium-magnesium carbonate (ACMC) accelerates
432 dolomitization at room temperature under abiotic conditions, Cryst. Growth Des. 20 (2020) 1434-
433 1441.
434 [28] T. Taut, R. Kleeberg, J. Bergmann, The new Seifert Rietveld program BGMN and its
435 application to quantitative phase analysis, Mater. Sci. (Bulletin of the Czech and Slovak

436 Crystallographic Association) 5 (1998) 55–64.
437 [29] G. Montes-Hernandez, et al., Sequential precipitation of a new goethite-calcite nanocomposite
438 and its possible application in the removal of toxic ions from polluted water, Chem. Eng. J. 214
439 (2013) 139-148.
440 [30] F. Renard, et al., Selenium incorporation into calcite and its effect on crystal growth: An
441 atomic force microscopy study, Chem. Geol. 340 (2013) 151-161.
442 [31] G. Montes-Hernandez, F. Renard, R. Lafay, Experimental assessment of CO_2-mineral-toxic
443 ion interactions in a simplified freshwater aquifer: Implications for CO_2 leakage from deep
444 geological storage, Environ. Sci. Technol. 47 (2013) 6247-6253.
445 [32] F. Renard, et al., Interactions of arsenic with calcite surfaces revealed by in-situ nanoscale
446 imaging, Geochim. Cosmochim. Acta 159 (2015) 61-79.
447 [33] A. Hamdouni, et al., Removal of Fe(II) from groundwater via aqueous portlandite carbonation
448 and calcite-solution interactions, Chem. Eng. J. 283 (2016) 404-411.
449 [34] F. Renard, et al., Sequestration of antimony on calcite observed by time-resolved nanoscale
450 Imaging, Environ. Sci. Technol. 52 (2018) 107-113.
451 [35] M. Grønlie Guren, et al., Direct imaging of coupled dissolution-precipitation and growth
452 processes on calcite exposed to chromium-rich fluids, Chem. Geol. 552 (2020) 119770.
453 [36] O. Giuffre, et al., Thermodynamic study on the interaction of ampicillin and amoxicillin with
454 Ca^{2+} in aqueous solution at different ionic strengths and temperatures, J. Chem. Eng. Data. 64
455 (2009) 800-809.
456 [37] G. Montes-Hernandez, et al., Formation of porous calcite mesocrystals from CO_2-H_2O-
457 $Ca(OH)_2$ slurry in the presence of common domestic drinks, CrystEngComm 17 (2005) 5725-5733.
458 [38] M. H. Zhang, Review on Fenton process for organic wastewater treatment based on

459 optimization perspective, Sci. Total Environ. 670 (2019) 110-121.

460 [39] I. Gozlan, A. Rotstein, D. Avisar, Amoxicillin-degradation products formed under controlled
461 environmental conditions: Identification and determination in the aquatic environment,
462 Chemosphere 91 (2013) 985-992.

463

Table 1. Summary of equilibrium parameters from Hill's model used to fit the data of the removal of antibiotics from water by portlandite aqueous carbonation and by nanomagnetite-interfacial Fenton reaction. Experimental isotherms were determined from breakthrough curves (Eq. 1).

Antibiotic	**Mineral**	**Parameters used to fit Hill's model**			$K_D=q_{e(max)}/K$ **L/g**	**Process**
		K **mg/L**	$q_{e(max)}$ **mg/g**	b		
Amoxicillin	Portlandite (1g)	30.62±0.22	9.48±0.03	5.84±0.27	0.30	Aqueous carbonation
Amoxicillin	Portlandite (2g)	29.74±0.36	8.35±0.09	9.32±1.35	0.28	Aqueous carbonation
Cefazolin	Portlandite (1g)	56.10±0.73	4.27±0.04	10.11±1.24	0.08	Aqueous carbonation
Ceftriaxone	Portlandite (1g)	66.59±0.49	2.69±0.02	16.43±1.81	0.04	Aqueous carbonation
Amoxicillin	Magnetite Nanoparticles (1g)	130.75±22.02	76.52±*	9.30±1.48	0.58	Fenton reaction

K: equilibrium concentration producing half-removed amount, $q_{e(max)}$: maximum removed amount, b: Hill's coefficient, K_D: liquid-solid distribution coefficient, *:very high error

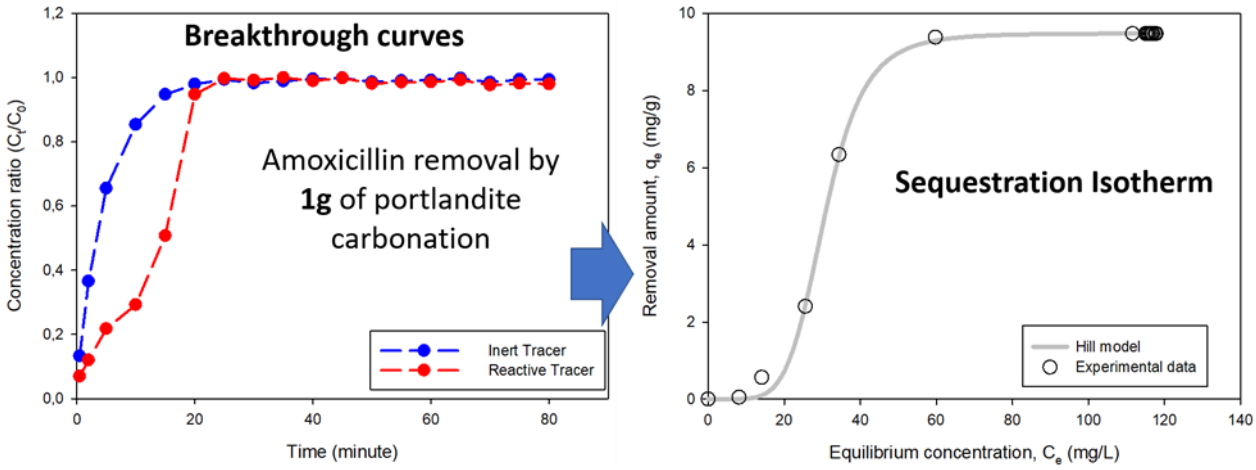

Figure 1. Removal of amoxicillin from CO_2-saturated solutions via portlandite carbonation. Left: Experimental breakthrough curves for inert tracer (reactor without portlandite) and reactive tracer (reactor with portlandite (1g)) (standard deviation<5% after equilibration of curves). Right: Amoxicillin removal isotherm from breakthrough curves determined by Eq. 1 and data fitted by Hill model (error of fitted parameters provided in Table 1).

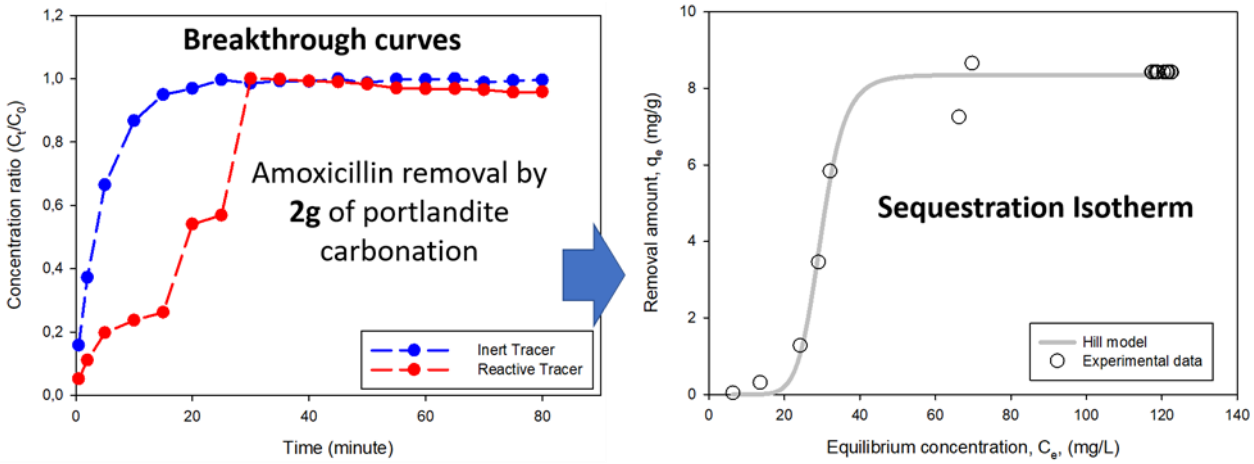

Figure 2. Removal of amoxicillin from CO_2-saturated solutions via portlandite carbonation. Left: Experimental breakthrough curves for inert tracer (reactor without portlandite) and reactive tracer (reactor with portlandite (2g)) (standard deviation<7% after equilibration of curves). Right: Amoxicillin removal isotherm from breakthrough curves determined by Eq. 1 and data fitted by Hill model (error of fitted parameters provided in Table 1).

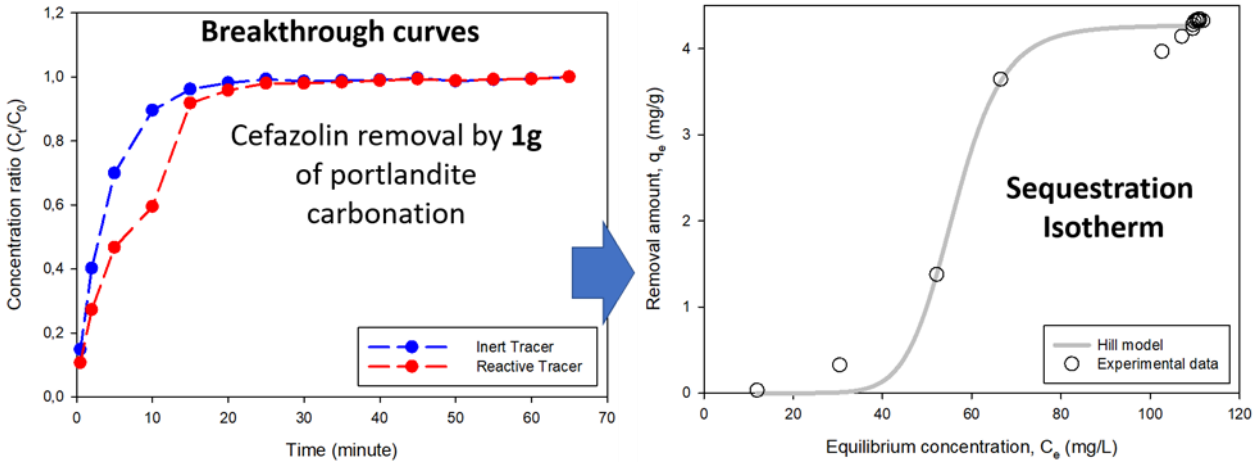

516

517

518

519

520

521

522

523 Figure 3. Left: Experimental breakthrough curves for inert tracer (reactor without portlandite) and
524 reactive tracer (reactor with portlandite (1g)) concerning cefazolin removal by aqueous carbonation
525 of portlandite ((standard deviation<5% after equilibration of curves). Right: Cefazolin removal
526 isotherm from breakthrough curves determined by Eq. 1 and data fitted by Hill model (error of
527 fitted parameters provided in Table 1).

528

529

530

531

532

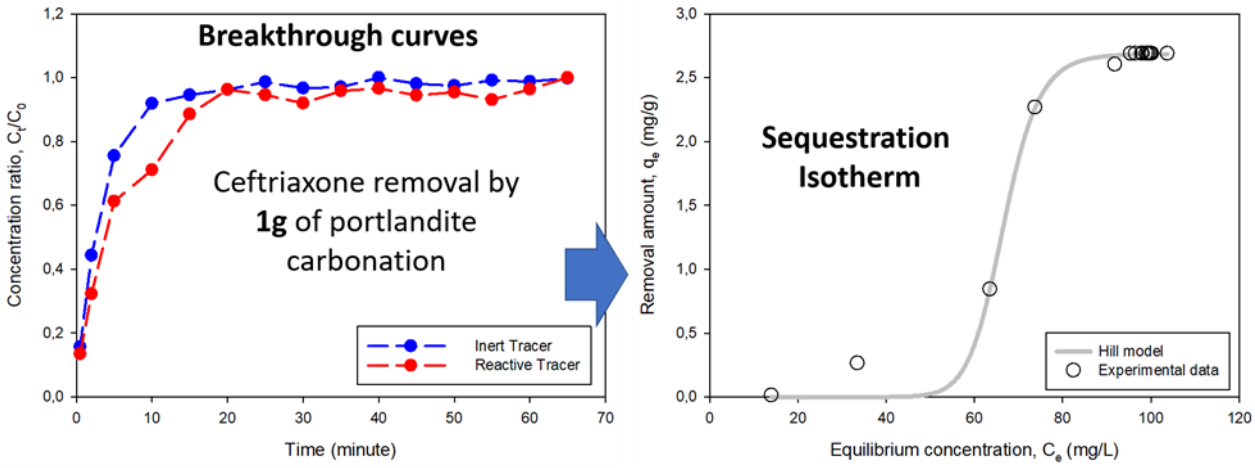

Figure 4. Left: Experimental breakthrough curves for inert tracer (reactor without portlandite) and reactive tracer (reactor with portlandite (1g)) concerning ceftriaxone removal by aqueous carbonation of portlandite (standard deviation<7% after equilibration of curves). Right: Ceftriaxone removal isotherm from breakthrough curves determined by Eq. 1 and data fitted by Hill model (error of fitted parameters provided in Table 1).

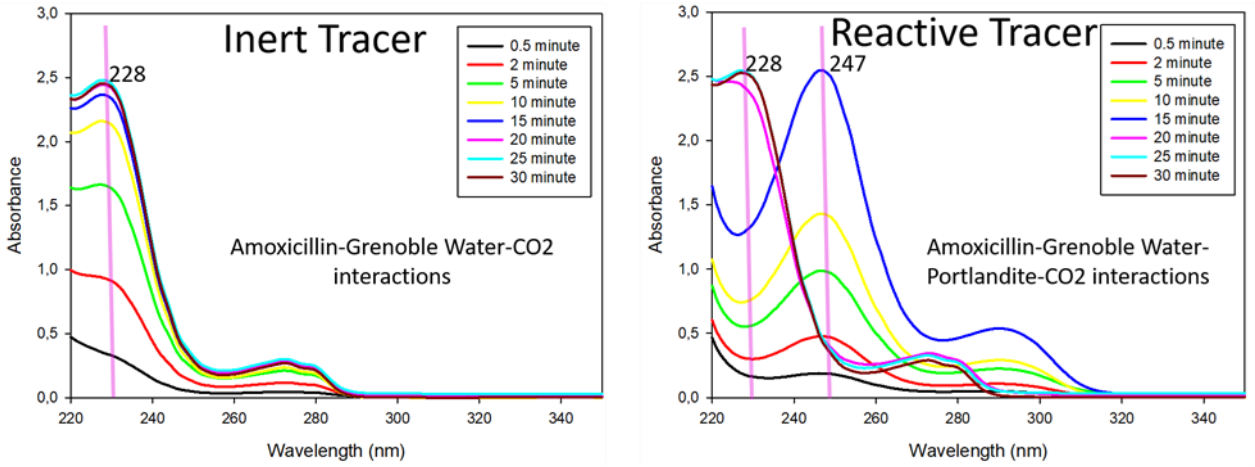

Figure 5. (Left) Time-lapse UV-Vis spectra for amoxicillin showing data from the inert tracer reactor in the percolation experiment. (Right) Time-lapse UV vis spectra for amoxicillin showing data from the reactive tracer reactor in the percolation experiment. Results indicate that amoxicillin is strongly complexed with calcium during carbonation process of portlandite (see reactive tracer reactor at right) because amoxicillin UV-Vis absorbance backs to typical absorbance when portlandite was completely consumed in the system.

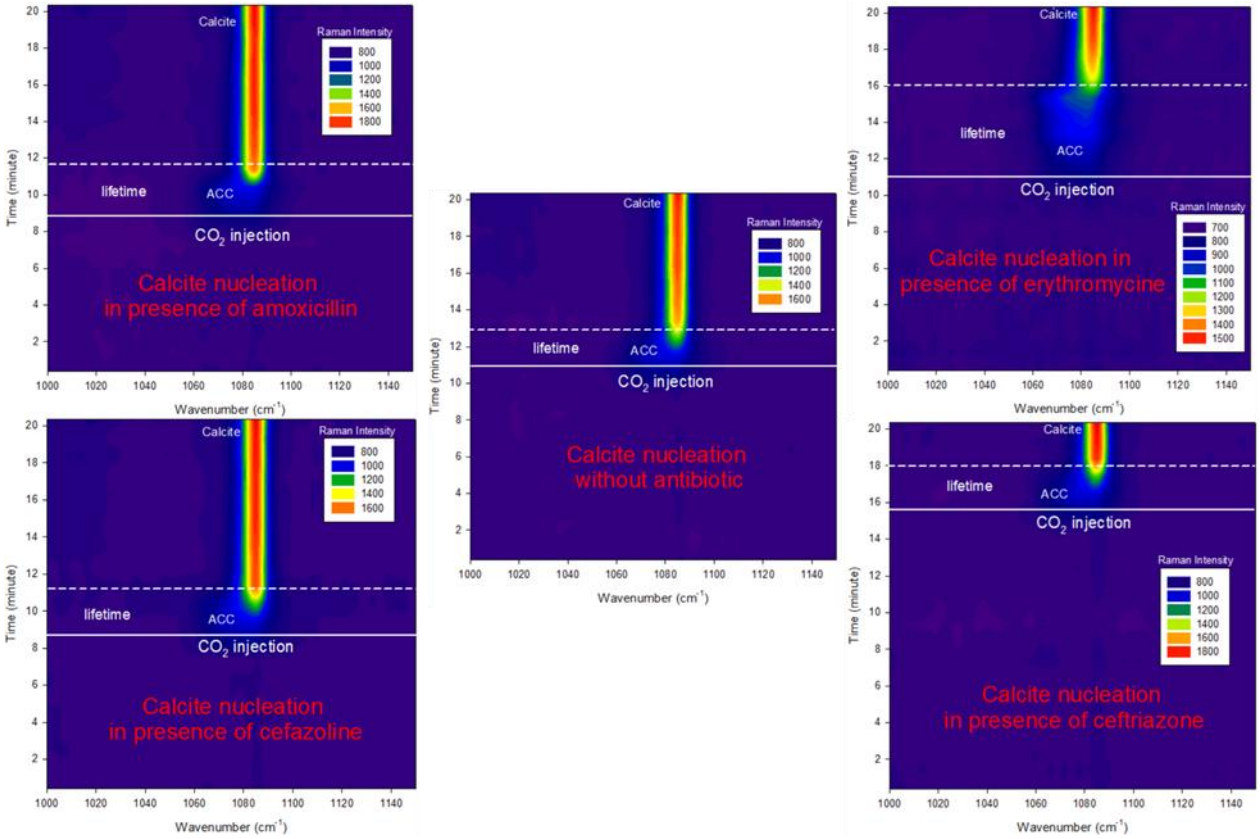

Figure 6. Time-lapse Raman spectra for calcite nucleation in presence of four different antibiotics, and reference without antibiotic. In all cases, amorphous calcium carbonate (ACC, blue halo on the figures) formed prior to calcite nucleation and was detected after the first minute of CO_2 injection. Its lifetime was similar and close to three minutes for all experiments, except in the presence of erythromycin where it was five minutes.

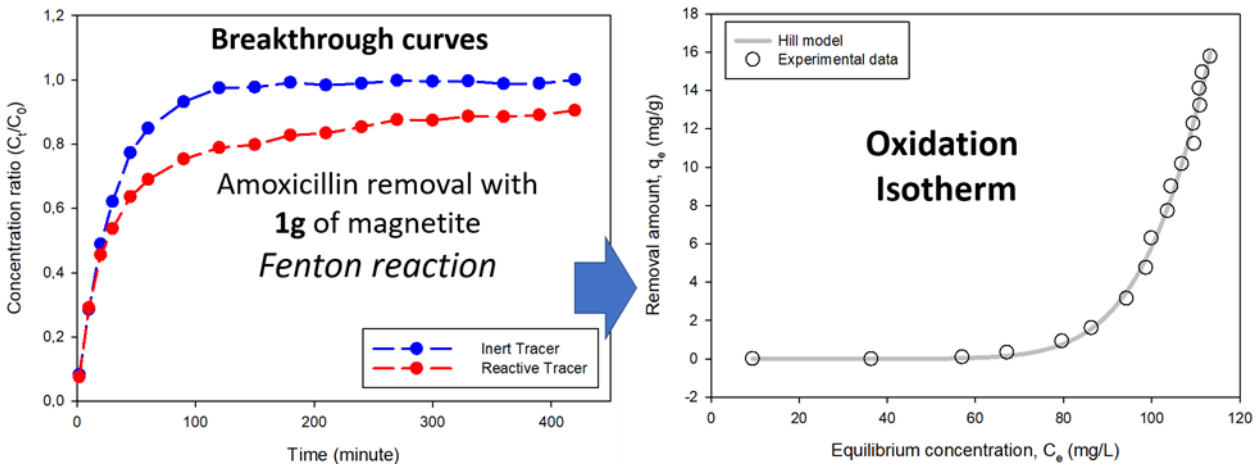

Figure 7. Left: Experimental breakthrough curves for inert tracer (reactor without magnetite) and reactive tracer (reactor with magnetite (1g)) during the removal of amoxicillin by aqueous magnetite-interfacial Fenton reaction (standard deviation<5% after equilibration of inert tracer curve). Right: Amoxicillin removal isotherm from breakthrough curves determined by Eq. 1 and data fitted with Hill's model (error of fitted parameters provided in Table 1).